Spin-Holstein Models in Trapped-Ion Systems

J. Knörzer,[1,2,*] T. Shi,[3,4,†] E. Demler,[5,6] and J. I. Cirac[1,2]
[1]*Max-Planck-Institute of Quantum Optics, Hans-Kopfermann-Straße 1, D-85748 Garching, Germany*
[2]*Munich Center for Quantum Science and Technology (MCQST), Schellingstraße 4, D-80799 München, Germany*
[3]*CAS Key Laboratory of Theoretical Physics, Institute of Theoretical Physics, Chinese Academy of Sciences, P.O. Box 2735, Beijing 100190, China*
[4]*CAS Center for Excellence in Topological Quantum Computation, University of Chinese Academy of Sciences, Beijing 100049, China*
[5]*Department of Physics, Harvard University, Cambridge, Massachusetts 02138, USA*
[6]*Institute for Theoretical Physics, ETH Zurich, 8093 Zurich, Switzerland*

(Received 16 September 2021; revised 29 December 2021; accepted 7 March 2022; published 25 March 2022)

In this work, we highlight how trapped-ion quantum systems can be used to study generalized Holstein models, and benchmark expensive numerical calculations. We study a particular *spin*-Holstein model that can be implemented with arrays of ions confined by individual microtraps, and that is closely related to the Holstein model of condensed matter physics, used to describe electron-phonon interactions. In contrast to earlier proposals, we focus on simulating many-electron systems and inspect the competition between charge-density wave order, fermion pairing, and phase separation. In our numerical study, we employ a combination of complementary approaches, based on non-Gaussian variational ansatz states and matrix product states, respectively. We demonstrate that this hybrid approach outperforms standard density-matrix renormalization group calculations.

DOI: 10.1103/PhysRevLett.128.120404

Electron-phonon interactions lie at the heart of several phenomena in condensed matter physics, including Cooper pairing [1] and the formation of polarons [2]. Generally, the low-energy excitations of electrons in solids are modified by their coupling to lattice vibrations, which alters their transport and thermodynamic behavior. Often simplified toy models can be employed to study those essential properties. As a complementary approach to traditional solid-state methods, quantum simulations utilize the rich toolbox of atomic physics to provide a characterization of equilibrium and dynamical properties of paradigmatic quantum many-body models.

The Holstein model is one such paradigmatic model that features a local coupling between the electron density and optical phonons on a lattice [3]. Despite its apparent simplicity, it hosts rich physics, giving rise to superconducting (SC) phases, charge-density wave (CDW) order and phase separation (PS) at strong coupling [4,5]. Yet, notwithstanding recent progress, its numerical treatment is often costly, especially when interactions become increasingly strong or of long-range character. As a tantalizing prospect, quantum simulators may help to gain new insights into the underlying physical mechanisms, and potential implementations include trapped ions [6,7], hybrid atom-ion systems [8], cold atoms [9], and quantum dots [10]. In trapped ions, their spin and motional degrees of freedom can be harnessed to realize a quantum-optics analog of the electron-phonon system [11–14], which enables access to a variety of system observables. Moreover, their key parameters may be tuned *in situ* to explore different regions of the phase diagram. Currently available setups may thus be utilized to improve and benchmark analog quantum simulators against state-of-the-art numerical methods. This paves a way toward the quantum simulation of even more complex electron-phonon models that could be implemented using trapped-ion setups.

In this Letter, we theoretically investigate such trapped-ion systems and derive an effective model that contains strong and highly nonlocal interactions between effective spins and lattice phonons. We highlight its similarities and differences with the Holstein model and develop a powerful numerical toolbox to thoroughly characterize its ground-state properties. Our numerical method combines density matrix renormalization group (DMRG) calculations [15,16] and computations based on non-Gaussian variational ansatz states (NGS) [17,18]. This hybrid approach is shown to particularly excel at studying the quantum many-body system at large spin-phonon couplings and large phonon numbers. We define spin and phonon observables motivated by the physics of the Holstein model and study their characteristics. Using these observables, we identify SC and CDW phases and their relation to the ion-trap

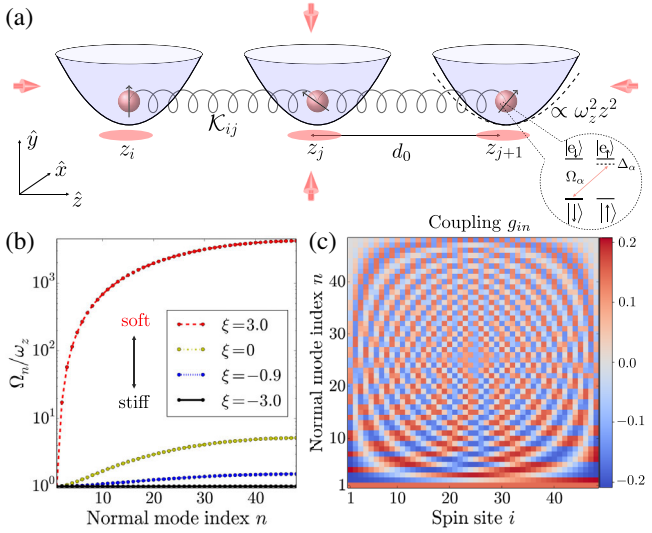

FIG. 1. Schematic illustration of setup. (a) Trapped-ion chain subject to three counterpropagating laser beams. The microtraps are aligned along the $\hat{z}$ direction at a distance d_0. Ions are coupled to each other via their mutual Coulomb interaction, indicated by springs. The inset shows an exemplary level scheme with four internal states $|\uparrow\rangle, |\downarrow\rangle, |e_\downarrow\rangle, |e_\uparrow\rangle$, and a σ^+ transition with laser parameters Ω_α and Δ_α. (b) Normal-mode frequencies Ω_n/ω_z for different values of ξ. ω_z is fixed while d_0 is varied. (c) Coupling g_{in} for $\xi = 0$ exemplarily shows long-range interactions between spins and phonons.

parameters, thus demonstrating the rich Holstein-like physics of the trapped-ion system. Finite-temperature and finite-size calculations show that our results can be expected to be robust against thermal excitations in state-of-the-art setups.

Setup and model.—We consider a physical system of N ions with mass m, each confined to a harmonic microtrap to guarantee an equidistant spacing of ions. All of the ions' equilibrium positions are assumed to be aligned along the $\hat{z}$ axis at a nearest-neighbor distance d_0, see Fig. 1(a). In a laser beam configuration which hosts three standing waves along the $\hat{x}$, $\hat{y}$, and $\hat{z}$ axes, light that is off resonant with chosen hyperfine-state transitions of the ions can be harnessed to introduce a coupling between the motional and spin degrees of freedom of all ions [11,12]. We assume large transverse trap frequencies and eliminate the motional degrees of freedom along $\hat{x}$ and $\hat{y}$ via a polaron transformation. As a result, pseudospins at a distance r become effectively coupled through an effective dipolar interaction J/r^3 at strength J. As outlined in more detail in Supplemental Material [19] we obtain an effective description of our system which takes the form

$$H_{\text{eff}} = \sum_n \Omega_n a_n^\dagger a_n + \sum_{\substack{i\neq j,\\ \alpha=x,y}} \frac{J}{|i-j|^3}\sigma_i^\alpha \sigma_j^\alpha + H_{\text{int}}, \quad (1)$$

where $a_{n=1,\ldots,N}$ are annihilation operators of the N collective phonon normal modes with frequencies Ω_n [see Fig. 1(b)], σ_i^α denotes the Pauli matrix associated with the internal spin states $|\uparrow\rangle$ and $|\downarrow\rangle$ at site i and direction α. In terms of the mode expansion $r_i = \sum_i g_{\text{in}}(a_n + a_n^\dagger)$ the interaction $H_{\text{int}} = -F_z \sum_i r_i(1+\sigma_i^z)$ of spins and local longitudinal phonons becomes

$$H_{\text{int}} = -F_z \sum_{i,n} g_{\text{in}}(a_n + a_n^\dagger)(1+\sigma_i^z), \quad (2)$$

where g_{in} describes the nonlocal coupling between phonon normal modes and spins [see Fig. 1(c)]. Here, we have made the Lamb-Dicke approximation, which can be justified in experiment if the light-induced coupling between internal spin states and motional states of the ions is sufficiently small.

Our effective model in Eq. (1) contains several key parameters that determine its behavior. In the following, we set $\omega_z/J = 1$ for all microtraps, and focus on the rich physics left to explore with the remaining free parameters. In particular, the system can now be described by (i) the spin-phonon coupling F_z and (ii) the ion trap stiffness $\beta = e^2/(m\omega_z^2 d_0^3)$ along the $\hat{z}$ direction. Throughout this work, we will use $\xi = \log\beta$. The limit $\xi \lesssim -1$ ($\xi \gtrsim 1$) is usually referred to as the stiff (soft) limit, in which the phonon dispersion is weak (strong) [see Fig. 1(b)]. The ion-trap setup allows us to switch between the adiabatic (small phonon frequency) and diabatic (large phonon frequency) regimes of the spin-Holstein model (1).

Numerical approach.—In our numerical study of Eq. (1), we complement DMRG simulations with calculations based on NGS, $|\Psi_{\text{NGS}}\rangle$, that can be written in the form [17]

$$|\Psi_{\text{NGS}}\rangle = U_S|\Psi_{\text{GS}}\rangle, \quad (3)$$

where U_S is a unitary operator and $|\Psi_{\text{GS}}\rangle$ an arbitrary Gaussian state, both of which depend on a set of variational parameters [19]. We derive and solve the equations of motion for these variational parameters to obtain the many-body ground state of H_{eff}, see [19] for more details. In order to treat the model in Eq. (1) with the NGS, we employ a Jordan-Wigner transformation and map H_{eff} onto a fermionic model via

$$\sigma_i^z = 2c_i^\dagger c_i - 1, \qquad \sigma_i^+ = e^{i\pi\sum_{l<i} c_l^\dagger c_l} c_i^\dagger. \quad (4)$$

Expressing the Hamiltonian (1) in terms of fermionic operators by means of (4) shows the similarity with the standard Holstein model, as studied in condensed matter physics. In this analogy, spin-spin interactions translate to electron hopping and spin-phonon to electron-phonon interaction. The differences between the standard Holstein model and our model (1) are the following: first, one key difference originates from the long-range hopping terms $\propto P_{ij}/|i-j|^3 c_i^\dagger c_j$ (with the string operator P_{ij}, see [19] for more details) present in our effective fermionic model, which stems from the dipolar decay of interactions in

Eq. (1). Second, in contrast to the genuine Holstein model which features a purely local coupling of electron and Einstein phonon, i.e., $g_{\mathrm{in}} = \delta_{\mathrm{in}}$ in Eq. (2), the phonon described by Eq. (1) is dispersive and its bandwidth may be tuned by means of ξ.

While NGS excel at numerical efficiency and capture the essential physics well, DMRG yields higher numerical accuracy. However, the DMRG study of Eq. (1) faces several technical challenges. Arguably two of the most relevant practical obstacles are associated with (i) not getting stuck in a local energy minimum during the algorithm, and (ii) avoiding truncation errors introduced by working with finite local phonon Hilbert spaces. In our numerical treatment, we find that (i) NGS can provide an excellent educated guess for the initial state fed into the DMRG algorithm, thus lowering the chances for getting stuck with a metastable solution. Moreover, (ii) the truncation error associated with finite local Hilbert spaces can be significantly lowered by employing a unitary displacement transformation on Eq. (1) (see [19]). Note that more general approaches exist to tackle this issue and have been applied to problems with fermion-phonon coupling [20–25].

Phase diagram.—As the spin-spin couplings and spin-phonon interactions compete, the many-body ground state displays several distinct phases as a function of phonon parameter ξ and spin-phonon coupling strength F_z. Equipped with our numerical toolbox, we study the ground-state properties of H_{eff} and calculate several spin and phonon observables. Especially, we introduce the CDW order parameter

$$O_{\mathrm{CDW}} = \frac{1}{2N}\sum_{n=1}^{N}(-1)^n(1+\langle\sigma_n^z\rangle), \tag{5}$$

and the four-point spin correlator

$$O_{\mathrm{SC}} = \langle\sigma_i^+\sigma_{i+1}^+\sigma_{i+\delta}^-\sigma_{i+1+\delta}^-\rangle, \tag{6}$$

with which we identify the superconducting ground state by calculating its decay as a function of δ for fixed i. The order parameters that we compute with the NGS approach for the fermionic model are derived in Supplemental Material [19].

We study the phase diagram for different filling factors $\nu = (\sum_i 1 + \langle\sigma_i^z\rangle)/(2N)$. In Fig. 2, we show the result for $N = 48$ spins at $\nu = 1/2$ (left panel) and $\nu = 1/4$ (right panel) as a function of F_z and ξ. The phase boundaries obtained with both numerical methods quantitatively agree with each other. Note that we focus here on the regime where $F_z \geq 1$ since there exists only a trivial Luttinger-liquid phase at small couplings.

At half filling ($\nu = 1/2$), and at sufficiently large spin-phonon coupling $F_z \gtrsim 1$, we find three distinct phases, that display charge-density wave order, quasi–long range superconducting order of p-wave pairing, and phase separation into two regions, in which the spins are pointing either up or down, respectively: (i) in the stiff limit ($\xi \lesssim -1$), where

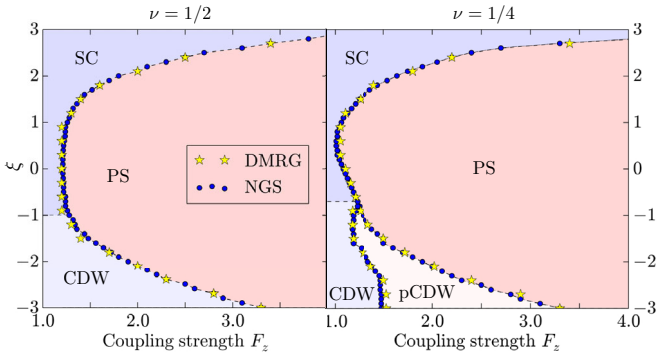

FIG. 2. Phase diagram of spin-Holstein model. $\xi \gtrsim 1$ ($\xi \lesssim -1$) corresponds to the soft (stiff) limit. Left panel: at filling factor $\nu = 1/2$, there exist three distinct phases at sufficiently large F_z, in a charge-density wave (CDW), a superconducting (SC), and a phase-separated (PS) regime. Right panel: at $\nu = 1/4$, there exists an additional PCDW phase (discussed in the main text). Numerical parameters: $N = 48$, $\omega_z/J = 1$.

the harmonic trapping potential dominates the Coulomb interaction, the phonons are more localized than in the soft limit. As a result, the phonon fluctuations around the ions' equilibrium position are suppressed, and in the regime $\xi \lesssim -1$ we discover a CDW state as the preferred ground state at moderate F_z. At half filling, the latter is characterized by an alternating spin configuration $\langle\sigma_n^z\rangle \propto (-1)^n$ ($n = 1, \ldots, N$) and a large order parameter $O_{\mathrm{CDW}} \sim 0.5$. (ii) In the soft limit ($\xi \gtrsim 1$), where the virtual phonon fluctuations are large and responsible for inducing attractive pairing interactions, we find a superconducting ground state that exhibits a slow power-law decay $O_{\mathrm{SC}} \sim \delta^{-\alpha}$, with $\alpha \approx 2$. (iii) There exists a competition between SC and CDW order, respectively, and phase separation. At sufficiently large coupling F_z, the spin-Holstein model displays an instability toward phase separation into two regions with opposite polarization, both in the stiff and in the soft limit.

At quarter filling ($\nu = 1/4$), we map out a similar phase diagram, and find an additional phase in the stiff limit ($\xi \lesssim -1$), which we refer to as the PCDW phase as shorthand notation for a phase that displays both phase separation and CDW order, see Fig. 2. It is prevalent at intermediate coupling strength, and it is characterized by the coexistence of phase separation and an enhanced CDW order parameter, with half of the spin chain being polarized and a staggered magnetization in the other half. Representative results for the spin configurations of different phases at $\nu = 1/4$ are shown in Figs. 3(e)–3(h). In all cases, we find excellent agreement between the DMRG and NGS numerical results.

Spin-phonon correlations.—To study the correlation between spins and phonons, we calculate the observable

$$\Pi_{ij} = \langle\sigma_i^z r_j\rangle - \langle\sigma_i^z\rangle\langle r_j\rangle. \tag{7}$$

In Figs. 3(a)–3(d) we show the DMRG results at $\nu = 1/4$ which agree very well with the corresponding results

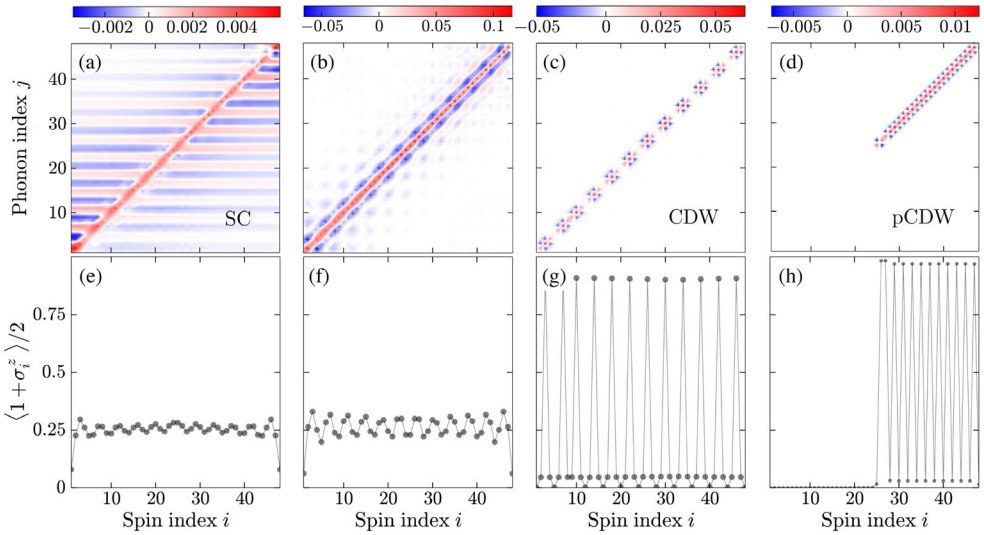

FIG. 3. Spin phonon correlator Π_{ij} and spin configuration for different ground states at quarter filling $\nu = 1/4$ as obtained with DMRG. Upper panel: spin-phonon correlator Π as defined in Eq. (7). Lower panel: site-dependent spin expectation value $(1 + \langle\sigma_i^z\rangle)/2$. The four columns correspond to particular choices for F_z and ξ (compare right panel of Fig. 2). (a) and (e): $F_z = 1.6$, $\xi = 2.1$ (SC regime). (b) and (f): $F_z = 0.6$, $\xi = -2.1$ (precursor of CDW regime). (c) and (g): $F_z = 1.2$, $\xi = -2.1$ (CDW regime). (d) and (h): $F_z = 1.5$, $\xi = -2.1$ (PCDW regime). Other numerical parameters: $N = 48$, $\omega_z/J = 1$.

obtained with the NGS. In the superconducting regime, cf. Fig. 3(a), the stripe pattern of Π_{ij} demonstrates the presence of nonlocal spin-phonon correlations. For a fixed spin index i, it displays oscillations with a period four near the center of the chain. In contrast, the correlations decay quickly in the CDW and PCDW regimes and are symmetric about $i = j$. In the stiff limit, at small couplings we find a precursor of the CDW state, where Π_{ij} decays more slowly away from $i = j$ than deep in the CDW regime, compare Figs. 3(b) and 3(c). A representative result for Π_{ij} for the PCDW ground state is shown in Fig. 3(d). As expected, the spin-phonon correlations vanish in one half of the system, while in the other they feature oscillations with a period two along the diagonal $i = j$, as would be expected for a CDW state at half filling. In the PCDW regime, the magnitude of the spin-phonon correlator is smaller than in the charge-density wave phase. At even larger F_z (phase separation), Π_{ij} vanishes almost everywhere, except for small contributions close to the domain wall.

Phonon numbers.—To characterize the phonon excitations, we decompose the phonon excitation number into the density of coherent phonons n_c and quantum fluctuations of the phonon density n_s:

$$n_c = \frac{1}{N}\sum_k |\langle a_k\rangle|^2, \qquad n_s = \frac{1}{N}\sum_k \langle a_k^\dagger a_k\rangle - n_c. \quad (8)$$

For Fig. 3, the average phonon numbers are (a) $n_c = 0.64$ and $n_s = 0.51$, (b) $n_c = 0.093$ and $n_s = 0.52$, (c) $n_c = 0.65$ and $n_s = 0.75$, (d) $n_c = 2.06$ and $n_s = 0.5$. When the system is in the SC phase, the virtual phonon fluctuations induce attractive interactions necessary for pairing, as familiar from BCS theory of superconductivity. In contrast, as the system enters the PCDW phase, the coherent phonon displacement becomes dominant. In the normal phase, the displacement is very small.

Experimental considerations.—Trapped-ion experiments benefit from well-developed readout techniques. Ions can be excited from one spin state to another with single-site resolution, and subsequent fluorescence imaging allows the extraction of local expectation values $\langle\sigma_i^z\rangle$. Repeated measurements at different sites enable access to spin-spin correlation functions like $\langle\sigma_i^z\sigma_j^z\rangle$ and O_{SC}. Spin-phonon correlations may be probed with only spin measurements and additional lasers that locally couple spins and phonons. All observables of our numerical study may thus be probed experimentally. Many recent experiments have demonstrated that trapped-ion quantum simulations of spin models are feasible, with system sizes comparable to those considered here [26,27].

While we have only shown numerical results for a system with $N = 48$ ions, we also study how the phase boundary in Fig. 2 shifts in the (F_z, ξ) plane with respect to the system size N using NGS. Deep in the stiff limit ($\xi = -3$), we find that there is no noticeable influence of the system size on the phase boundaries both at half and quarter filling factors. However, in the soft limit, we find that the phase boundary moves to smaller (larger) F_z as N is increased (decreased). For example, at $\nu = 1/2$ and $\xi = 3$, we find the SC-to-PS transition near $F_z = 2.6$ for $N = 96$ and $F_z = 4.5$ for $N = 48$, while for $N = 24$, the phase boundary disappears, i.e., we do not find any critical point numerically for $F_z \leq 16$. For larger systems and in the soft limit, smaller coupling strengths are thus sufficient to induce phase separation. A scaling analysis of the NGS results obtained for systems

with up to $N = 400$ shows that the SC phase survives in the thermodynamic limit. For example, at $\xi = 3$ the SC-to-PS boundary moves to $F_z \approx 1$ for $N \to \infty$.

We perform finite-temperature calculations using the NGS to confirm that the predicted phases survive at $T > 0$ and may actually be observed in state-of-the-art experiments. At temperatures up to $T \sim J/k_B$, we find that the $T = 0$ ground states are robust and the phase diagrams in Fig. 2 change only insignificantly. For $^{40}Ca^+$ ions at an effective temperature $T = 1\ \mu$K and with our choice $\omega_z/J = 1$, this corresponds to trap distances $d_0 \approx 5\ \mu$m deep in the soft limit ($\xi = 3$) and larger separations in the stiff limit. This shows that our results are consistent with the parameters of typical trapped-ion setups.

Conclusions.—To conclude, we have studied a generalized Holstein model that can be implemented in state-of-the-art trapped-ion experiments. In our numerical study, we have demonstrated that it can be useful to choose a hybrid approach in which calculations based on non-Gaussian variational ansatz states and density-matrix renormalization group complement each other. This allowed us to map out the phase diagram of the trapped-ion spin system, which is governed solely by tunable laser and ion trap parameters. While we have concentrated on $\nu = 1/2$ and $\nu = 1/4$, other filling factors may be explored in future work, and could give rise to an even richer hierarchy of phases in the stiff limit. As a future prospect, also more exotic models could be investigated that include higher-order interactions between phonons and spins. While they would be harder to tackle with classical methods, in a trapped-ion quantum simulator, they may be implemented by driving higher-order sidebands with a laser. In that way, the quantum simulator may possibly be operated in two regimes, one which is also accessible with classical calculations, and another that may go beyond what is achievable with state-of-the-art numerics. A straightforward extension of our work is the consideration of well-established Paul trap setups instead of microtrap arrays, in which the ions are not perfectly equidistantly spaced.

J. K. and J. I. C. acknowledge support from the Deutsche Forschungsgemeinschaft (DFG, German Research Foundation) under Germany's Excellence Strategy—EXC-2111–390814868. T. S. is supported by the NSFC (Grant No. 11974363). E. D. acknowledges support from the ARO Grant No. W911NF-20-1-0163, the AFOSR-MURI Grant No. FA95501610323, and the NSF EAGER-QAC-QSA Grant No. 2222-206-2014111. J. K. thanks Miles Stoudenmire for useful discussions.

J. K. and T. S. contributed equally to this work.

*johannes.knoerzer@eth-its.ethz.ch
†tshi@itp.ac.cn

[1] L. N. Cooper, Phys. Rev. **104**, 1189 (1956).
[2] H. Fröhlich, Adv. Phys. **3**, 325 (1954).
[3] T. Holstein, Ann. Phys. (N.Y.) **8**, 325 (1959).
[4] R. T. Scalettar, N. E. Bickers, and D. J. Scalapino, Phys. Rev. B **40**, 197 (1989).
[5] F. Marsiglio, Phys. Rev. B **42**, 2416 (1990).
[6] J. I. Cirac and P. Zoller, Nat. Phys. **8**, 264 (2012).
[7] R. Blatt and C. F. Roos, Nat. Phys. **8**, 277 (2012).
[8] U. Bissbort, D. Cocks, A. Negretti, Z. Idziaszek, T. Calarco, F. Schmidt-Kaler, W. Hofstetter, and R. Gerritsma, Phys. Rev. Lett. **111**, 080501 (2013).
[9] D. Gonzalez-Cuadra, P. R. Grzybowski, A. Dauphin, and M. Lewenstein, Phys. Rev. Lett. **121**, 090402 (2018).
[10] U. Bhattacharya, T. Graß, A. Bachtold, M. Lewenstein, and F. Pistolesi, arXiv:2106.09418.
[11] D. Porras and J. I. Cirac, Phys. Rev. Lett. **92**, 207901 (2004).
[12] X.-L. Deng, D. Porras, and J. I. Cirac, Phys. Rev. A **72**, 063407 (2005).
[13] V. M. Stojanovic, T. Shi, C. Bruder, and J. I. Cirac, Phys. Rev. Lett. **109**, 250501 (2012).
[14] K. Jachymski and A. Negretti, Phys. Rev. Research **2**, 033326 (2020).
[15] S. R. White, Phys. Rev. Lett. **69**, 2863 (1992).
[16] M. Fishman, S. R. White, and E. M. Stoudenmire, arXiv:2007.14822.
[17] T. Shi, E. Demler, and J. I. Cirac, Ann. Phys. (Amsterdam) **390**, 245 (2018).
[18] T. Shi, E. Demler, and J. I. Cirac, Phys. Rev. Lett. **125**, 180602 (2020).
[19] See Supplemental Material at http://link.aps.org/supplemental/10.1103/PhysRevLett.128.120404 for further details of the analytical derivations and numerical methods.
[20] E. Jeckelmann and S. R. White, Phys. Rev. B **57**, 6376 (1998).
[21] C. Zhang, E. Jeckelmann, and S. R. White, Phys. Rev. Lett. **80**, 2661 (1998).
[22] C. Guo, A. Weichselbaum, J. von Delft, and M. Vojta, Phys. Rev. Lett. **108**, 160401 (2012).
[23] C. Brockt, F. Dorfner, L. Vidmar, F. Heidrich-Meisner, and E. Jeckelmann, Phys. Rev. B **92**, 241106(R) (2015).
[24] J. Stolpp, J. Herbrych, F. Dorfner, E. Dagotto, and F. Heidrich-Meisner, Phys. Rev. B **101**, 035134 (2020).
[25] T. Köhler, J. Stolpp, and S. Paeckel, SciPost Phys. **10**, 058 (2021).
[26] J. Zhang, G. Pagano, P. Hess, A. Kyprianidis, P. Becker, H. Kaplan, A. V. Gorshkov, Z.-X. Gong, and C. Monroe, Nature (London) **551**, 601 (2017).
[27] C. Monroe, W. C. Campbell, L.-M. Duan, Z.-X. Gong, A. V. Gorshkov, P. W. Hess, R. Islam, K. Kim, N. M. Linke, G. Pagano, P. Richerme, C. Senko, and N. Y. Yao, Rev. Mod. Phys. **93**, 025001 (2021).